

In silico drug repositioning against human NRP1 to block SARS-CoV-2 host entry

Şeref GÜL^{1,2,*} ¹Department of Chemical and Biological Engineering, Koç University, İstanbul, Turkey²Biotechnology Division, Department of Biology, Faculty of Science, İstanbul University, İstanbul, Turkey

Received: 17.12.2020 • Accepted/Published Online: 08.05.2021 • Final Version: 30.08.2021

Abstract: Despite COVID-19 turned into a pandemic, no approved drug for the treatment or globally available vaccine is out yet. In such a global emergency, drug repurposing approach that bypasses a costly and long-time demanding drug discovery process is an effective way in search of finding drugs for the COVID-19 treatment. Recent studies showed that SARS-CoV-2 uses neuropilin-1 (NRP1) for host entry. Here we took advantage of structural information of the NRP1 in complex with C-terminal of spike (S) protein of SARS-CoV-2 to identify drugs that may inhibit NRP1 and S protein interaction. U.S. Food and Drug Administration (FDA) approved drugs were screened using docking simulations. Among top drugs, well-tolerated drugs were selected for further analysis. Molecular dynamics (MD) simulations of drugs-NRP1 complexes were run for 100 ns to assess the persistency of binding. MM/GBSA calculations from MD simulations showed that eltrombopag, glimepiride, sitagliptin, dutasteride, and ergotamine stably and strongly bind to NRP1. In silico Alanine scanning analysis revealed that Tyr²⁹⁷, Trp³⁰¹, and Tyr³⁵³ amino acids of NRP1 are critical for drug binding. Validating the effect of drugs analyzed in this paper by experimental studies and clinical trials will expedite the drug discovery process for COVID-19.

Key words: SARS-CoV-2, COVID-19, NRP1, drug repositioning, eltrombopag, sitagliptin

1. Introduction

Severe acute respiratory syndrome coronavirus 2 (SARS-CoV-2) infected over 40 million people and resulted in more than 1.5 million deaths around the world since December 2019.¹ The coronavirus disease-2019 (COVID-19) has symptoms of pneumonia manifesting fever, fatigue, dyspnea, chest pain, and cough which are also observed in other viral respiratory diseases (Yi et al., 2020). The whole-genome analysis showed that SARS-CoV-2 belongs to the *Betacoronavirus* genera and has a 96% genomic sequence identity to that of bat coronavirus (Wu et al., 2020b; Zhou et al., 2020). Despite the high genomic similarities, SARS-CoV-2 behaves more aggressively than SARS-CoV in terms of viral load, reaching the peak RNA concentration, tissue tropism, and transmission efficiency (Wolfel et al., 2020).

SARS-CoV-2 genome is composed of a (+) sense single-strand RNA (ssRNA) with 14 open reading frames (ORFs). SARS-CoV-2 synthesizes two polyproteins, ORF1a and ORF1ab, and four structural proteins e.g., spike (S), envelop (E), matrix (M), and nucleocapsid (N)

¹Worldometers (2020). COVID-19 Coronavirus Pandemic [online]. Website: <https://www.worldometers.info/coronavirus/> [accessed 05 December 2020].

proteins and accessory proteins (3a, 3b, p6, 7a, 7b, 8b, 9b, and orf14) (Wu et al., 2020a; Yoshimoto, 2020). Proteolytic cleavage of ORF1a and ORF1ab by proteases leads to the production of 16 nonstructural proteins (nsps). Among nsps, nsp5 (3C-like protease, 3CL^{pro}) first cleaves its bounds with nsp4 and nsp6, then cleaves the ORF1a and ORF1ab at 11 sites (Du et al., 2004; Muramatsu et al., 2013). Besides 3CL^{pro}, nsp3 (papain-like protease, PL^{pro}) cleaves these polyproteins at three sites and completes the production of 16 nsps (Baez-Santos et al., 2015; Thiel et al., 2003).

S protein of SARS-CoV-2 interacts with angiotensin-converting enzyme 2 (ACE2) that has been accepted as the main receptor for the entry of the virus (Wang et al., 2020; Yan et al., 2020). ACE2, a membrane protein, is expressed in lung, upper and stratified epithelial cells of the esophagus, heart, kidney, testis, colon, ileum, and intestine (Donoghue et al., 2000; Zhang et al., 2020). Despite the attenuated expression of ACE2 in elderly people, increased or unaffected severity of COVID-19 symptoms (Walls et al., 2020) in these people (Liu et al., 2020; Omori et al., 2020; Singh et al., 2020a), and high viral loads in the throat (Wolfel et al., 2020) suggest the existence of an alternative receptor for the virus entry.

* Correspondence: serefgul@ku.edu.tr

A polybasic sequence (Arg⁶⁸²Arg-Ala-Arg⁶⁸⁵) at the S1/S2 region of S protein of the SARS-CoV-2 may explain its higher transmission rate and tissue tropism. This sequence is also conserved in the S protein of various pathogenic human viruses such as Ebola, influenza, and HIV-1 (Tse et al., 2014). Cleavage of the S protein within the polybasic sequence, which is primed by transmembrane serine protease 2 (TMPRSS2) via furin produces S1 and S2 (Hoffmann et al., 2020b). *FURIN* mediated cleavage of S protein results in increased tropism and the infection rate of SARS-CoV-2, most probably because of the formation of new cell surface binding regions (Hoffmann et al., 2020a; Wrapp et al., 2020). Knocking down *FURIN* gene or using its inhibitor decreases the virus entry to cells and syncytia formation in the infected cells, respectively (Shang et al., 2020; Walls et al., 2020).

(Arg⁶⁸²Arg-Ala-Arg⁶⁸⁵) sequence is aligned with [R/K]XX[R/K] motif (R: arginine, K: lysine, and X is any amino acid), named as C-end rule (CendR). CendR binds and activates cell surface receptors neuropilin (NRP1,2) (Teesalu et al., 2009). NRP1 binds to several growth factors such as vascular endothelial growth factors (VEGFs) (Soker et al., 1998), hepatocyte growth factor (Sulpice et al., 2008), and transforming growth factor (Cao et al., 2010). Among those, the interaction between NRP1 and VEGF-A₁₆₅ has been extensively studied (Teesalu et al., 2009; Jarvis et al., 2010; Parker et al., 2012; Fantin et al., 2014; Jia et al., 2014; Mota et al., 2018; Powell et al., 2018). C-terminal arginine residue and CendR motif of VEGF-A₁₆₅ critically interact with b1 domain of NRP1 (NRP1-b1) in which natural and artificial NRP1 inhibitors were explored (Vander Kooi et al., 2007). Having a cavity on CendR binding pocket of NRP1 made it an attractive target for designing small-molecules. Several molecules blocking NRP1-VEGF interaction were developed (Jarvis et al., 2010; Powell et al., 2018). First designed NRP1 inhibitor, EG00229, occupied the VEGF-A binding region by directly interacting with Tyr²⁹⁷, Glu³⁴⁸, Thr³⁴⁹, and Tyr³⁵³ (Jarvis et al., 2010). Based on the discovered scaffold of EG00229, a more potent molecule, EG01377 was developed (Powell et al., 2018). Both these molecules bind to NRP1 with a very similar mode.

Recent studies showed that interaction between NRP1 and protein S of SARS-CoV-2 is required for the SARS-CoV-2 cell entry (Cantuti-Castelvetri et al., 2020; Daly et al., 2020). While coexpression of NRP1 with ACE2 and TMPRSS2 increased the infection, monoclonal antibody targeting the b1b2 extracellular domain of NRP1 significantly inhibited the infection. The stimulating effect of NRP1 on the virus infection diminished when the furin cleavage site of SARS-CoV-2 is mutated (Cantuti-Castelvetri et al., 2020). Analysis of direct interaction

between CendR peptide of protein S and NRP1 using isothermal titration calorimetry method showed that binding affinity of the complex is between 20 and 13 μ M depending on the pH. Mutating the critical arginine residue (Arg⁶⁸⁵) on the CendR of protein S prevented the NRP1 binding (Daly et al., 2020). The crystallographic analysis confirmed that the binding mode of protein S' CendR to the NRP1 is similar to the previously resolved NRP1-VEGF-A structure (Daly et al., 2020; Parker et al., 2012).

To date, there is no consensus on the treatment of COVID-19 yet. Since developing a new drug is costly and requiring a long period, repurposing of U.S. Food and Drug Administration (FDA) approved drugs may provide an alternative approach to find a therapeutic for the COVID-19 treatment within a reasonable time and cost. Multiple targets are available to neutralize COVID-19. For example, virus entry proteins on the host (ACE2, TMPRSS2, NRP1), replication machinery of the virus (3CL^{Pro} RNA-dependent RNA polymerase), virus proteins taking roles on the assembly mechanism (protein E) and the release of the virus (protein M and N) are candidates for drug development and drug repurposing (Venkatagopalan et al., 2015; Schoeman and Fielding, 2019; Li et al., 2020a; Sarma et al., 2020). Given the crucial role of NRP1 for the SARS-CoV-2 entry into the host specifically in elderly people, this in silico study aimed to repurpose FDA-approved drugs against b1 domain of NRP1 to find a promising drug to block SARS-CoV-2 infection. For this purpose, initially docking simulations were run to find drugs with high binding affinity to b1 domain of NRP1. As a control, previously identified NRP1 inhibitor, EG01377, was docked to the same pocket. While docking binding energy of the inhibitor is around -6.0 kcal/mol, over 250 drugs have -7.4kcal/mol or lower AutoDock Vina binding energy. Drugs were sorted based on docking binding energies, and an extensive literature search was done to select well-tolerated drugs for further analysis. One hundred ns molecular dynamics simulations (MD) of drug-NRP1 complexes showed that thrombopoietin receptor agonist eltrombopag, migraine drug ergotamine, drugs for type 2 diabetes sitagliptin and glimepiride, and antiandrogen dutasteride can stably interact with NRP1. Crystal structure of NRP1 in complex with EG01377 (PDB ID: 6FMF) was simulated to compare the affinity of selected drugs with its inhibitor. Binding free energy calculation using MM/GBSA method showed that selected drugs have a comparable or better affinity to NRP1 than EG01377. Alanine scanning calculations revealed Tyr²⁹⁷, Trp³⁰¹, and Tyr³⁵³ as the critical amino acid residues for drug-NRP1 interaction. These findings may be used in experimental studies and clinical trials to test the effect of promising

drugs alone or in combination with current COVID-19 treatment protocols.

2. Materials and methods

High-resolution human NRP1 structure (PDB ID: 6FMC) was retrieved from The Protein Data Bank² (Powell et al., 2018). Protein was prepared for docking simulations via Dock Prep module of UCSF Chimera as described previously (Tardu et al., 2016; Doruk et al., 2020; Gul et al., 2020). Crystal water molecules were removed and if alternate locations are available for residues, the ones with the higher occupancies were selected. Rotamer library developed by Shapovalov and Dunbrack (2011) was used to complete missing side chains of amino acids, polar hydrogens were added, and nonpolar hydrogens were merged with bound atoms. Atom charges should be defined to run docking simulations. Thus, Gasteiger charges to each atom in the protein were assigned using Auto Dock Tools (ADT) (v. 1.5.6). Structures of drugs were downloaded from Zinc15 database catalogue of FDA-approved drugs. Set of drugs used in this study were imported from the U.S. Environmental Protection Agency's (EPA) distributed structure-searchable toxicity (DSSTox) database. The 3948 drugs and NRP1 inhibitor (EG01377) were prepared for docking by using ADT suite. Inhibitor binding pocket of NRP1 was targeted for docking simulations in which grid center was placed on the center of Tyr²⁹⁷, Glu³⁴⁸, and Tyr³⁵³ side chains with 6400 Å³ of the grid box. AutoDock Vina (version 1.1.2) was used for the docking (Trott and Olson, 2010).

With the aid of VMD, NRP1 structure (PDB ID: 6FMF) was solvated using TIP3P water molecules in a rectangular box with edge lengths of $x = 75 \text{ \AA}$, $y = 80 \text{ \AA}$, $z = 75 \text{ \AA}$ and a size of $4.50 \times 10^5 \text{ \AA}^3$. Solvated protein was neutralized and then ionized with sodium-chloride salt (Na^+ and Cl^-) to 150 mM final concentration to mimic the physiological conditions (Humphrey et al., 1996). Twenty thousand steps of energy minimization (via conjugate gradient) was performed. The minimized system was gradually heated and then equilibrated for 1.4 ns (NPT ensemble) with constraints on the protein. Constrains starting from 2 kcal/mol/Å² were reduced by 0.5 kcal/mol/Å² for each 0.4 ns equilibration run. Production simulation of 100 ns for each equilibrated drug-NRP1 complex was run using 2 fs time step at 310K and 1atm pressure. Langevin thermostat and Langevin barostat maintained the temperature and pressure, respectively. To calculate the force acting on the system van der Waals (12Å cut-off) and long-range electrostatic interactions (via particle-mesh Ewald) were

²RCSB PDB (Research Collaboratory for Structural Bioinformatics PDB) (2021). The Protein Data Bank [online]. Website www.rcsb.org [accessed 18 September 2020].

calculated. NAMD (Phillips et al., 2005) software and CHARMM36m force field (Huang et al., 2017) were used for all MD simulations. CHARMM-GUI server was used to generate parameters of drugs (Jo et al., 2008; Kim et al., 2017).

Analyses of protein-drug interactions were done by following these steps: 1) MD trajectory of each drug-protein simulation was visualized to inspect the position of the drug. If the drug leaves the binding pocket, that one is eliminated. 2) For simulations that drug-protein interaction was maintained for 100 ns, root mean square deviation (RMSD) of C_α atoms was calculated to verify the successful equilibration of the system. 3) Contact frequency between drug and nearby amino acid residues were carried out for determining the binding residues. 4) Binding free energy (BFE) of drugs was calculated using molecular mechanics generalized born surface area (MM/GBSA) method. 5) Amino acid residue with a high contact frequency was mutated to Alanine to calculate their contribution to BFE of drugs. All MD analyses were performed and protein figures were prepared by using VMD and Pymol, respectively (Humphrey et al., 1996; DeLano, 2009). RMSD trajectory tool and timeline function in VMD were used to calculate RMSD of protein and contact frequencies between drug and protein, respectively. Unstructured and highly dynamic first 9 N-terminal amino acid residues were excluded from the RMSD calculation.

For MM/GBSA and Alanine scanning calculations, MMPBSA.py script of AmberTools20 was used (Case et al., 2020). For each calculation, 25,000 frames from 100 ns simulations were used. BFE between drug and protein is calculated based on Equation 1:

$$\Delta G_{\text{binding}} = G_{\text{complex}} - G_{\text{receptor}} - G_{\text{ligand}} \quad (1)$$

G_{complex} : Energy of protein-drug complex,
 G_{receptor} : Energy of protein only,
 G_{ligand} : Energy of unbound drug.

3. Results

To discover an antiviral drug diverse targets are available from viral replication enzymes to host proteins facilitating the virus entry and to proteins responsible for the virus release (Boopathi et al., 2020; Lo et al., 2020; Wu et al., 2020b). Several in silico and in vivo drug repurposing studies are carried out using proteases (3CL^{pro} and PL^{pro}) and RNA-dependent RNA polymerase (RdRp) of SARS-CoV-2 as targets (Bharadwaj et al., 2020; Ghosh et al., 2020; Gul et al., 2020; Li et al., 2020c; Wang, 2020). In addition, host proteins TMPRSS2 and ACE2 which primes protein S and mediates SARS-CoV-2 entry to host, respectively, are targeted for drug repositioning as well (Bagheri and

Niavarani, 2020; Busnadiego et al., 2020; Carino et al., 2020; Choudhary et al., 2020; DurdaGi, 2020; Kumar et al., 2020; Singh et al., 2020b).

NRP1 is a recently identified receptor that facilitates the SARS-CoV-2 cell entry in coordination with ACE2 and TMPRSS2 (Cantuti-Castelvetri et al., 2020; Daly et al., 2020). S protein of SARS-CoV-2 attaches to the host cells for the virus entry (Wang et al., 2020; Yan et al., 2020). When the S protein is cleaved by the host protease, S1 and S2 proteins are generated. S1 has a polybasic sequence (Arg⁶⁸²-Arg-Ala-Arg⁶⁸⁵) at the C-terminal which interacts with b1 domain of NRP1 (Cantuti-Castelvetri et al., 2020; Daly et al., 2020) (Figure 1). Mutating the critical Arg⁶⁸⁵ diminishes protein S and NRP1 binding (Daly et al., 2020) and antibody against b1b2 domain of NRP1 relieve the SARS-CoV-2 infection (Cantuti-Castelvetri et al., 2020). Drugs having a high affinity to CendR binding pocket of NRP1 can be used in the COVID-19 treatment by blocking SARS-CoV-2 entry into cells.

3.1. Docking simulations

AutoDock Vina program was used to calculate binding energy and predict the binding mode of drugs to the target pocket as described before (Tardu et al., 2016; Gul et al., 2020). During the docking simulations, receptor (NRP1) was treated as a rigid body and drugs were allowed to sample different conformations in the CendR binding

pocket. NRP1 inhibitor, EG01377 (Powell et al., 2018), was docked to NRP1 as a control to evaluate the binding affinities of drugs against NRP1. Vina binding energy of EG01377 was calculated as -6.0 kcal/mol (Table 1). The docked conformation of EG01377 is in contact with Tyr²⁹⁷, Trp³⁰¹, Lys³⁵¹, and Tyr³⁵³ similar to observed in the crystal structure (6FMF) (Figure 2A). Docking simulations revealed that over 100 molecules have Vina binding energies -7.6 kcal/mol or lower (Table S1). Histogram representation of Vina binding energies of all drugs are provided in (Figure S1). Top 15 of those drugs having the Vina binding energies between -8.5 and -8.0 kcal/mol were given in (Table 1) with their ZINC IDs, structures, and types.

Docking simulations showed that, according to the descriptions in DrugBank (Wishart et al., 2006), various types of drugs such as anticancer, antipsychotics, antiinflammatory, antibiotics, antidiabetics, and estrogen hormone may bind to NRP1 (Table S1). For further analysis, widely used drugs eltrombopag (-8.5 kcal/mol), glimepiride (-8.2 kcal/mol), dutasteride (-8.2 kcal/mol), sitagliptin (-8.2 kcal/mol), ergotamine (-8.1 kcal/mol) at the top of the docking result list, and two antimalarial drugs, mefloquine (-8.0 kcal/mol) and atovaquone (-7.9 kcal/mol), having similar binding energies to top drugs were selected. Two-dimensional diagram of interaction

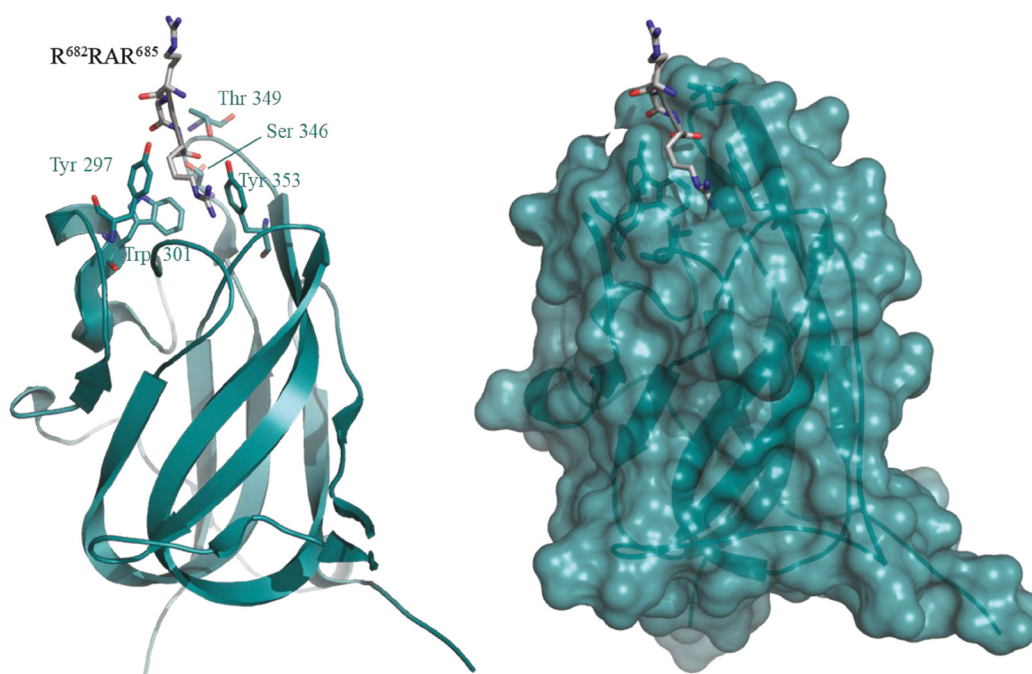


Figure 1. Structure of NRP1 in complex with polybasic peptide at the C-terminal of protein S (PDB ID: 7JJC). NRP1 is shown in cartoon at left critical residues are shown in ball and sticks (cyan color), polybasic peptide is shown in ball and sticks (gray color) representation. NRP1 is shown in surface representation at right.

Table 1. List of top 15 drugs having the best binding affinity to NRP1 inhibitors.

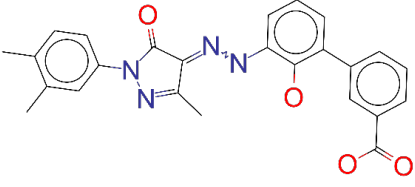
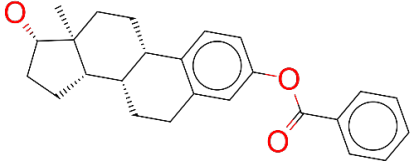
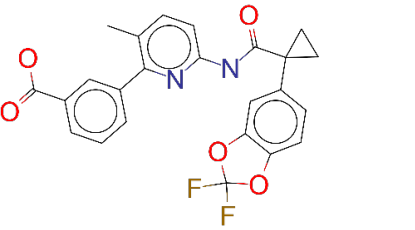
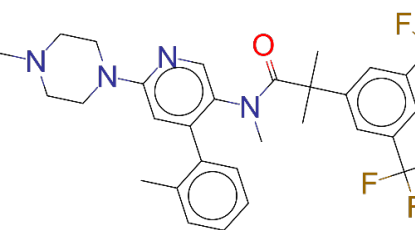
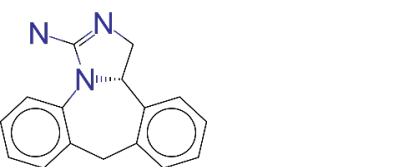
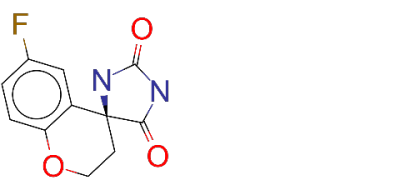
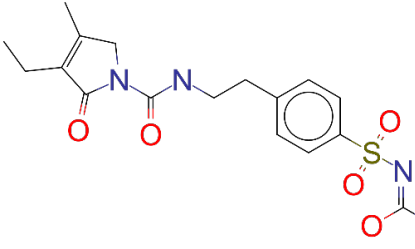
ZINC ID and/or drug name	2D Structure	Vina binding affinity (kcal/mol)	Type
ZINC000011679756/ Eltrombopag		-8.5	Thrombopoietin receptor agonist
ZINC000003830767/ Estradiol benzoate		-8.5	Estrogenic steroids
ZINC000064033452/ Lumacaftor		-8.4	Used to treat fibrosis (CF) in patients having homozygous F508del mutation in their CFTR gene.
ZINC000011681563/ Netupitant		-8.3	Antiemetic
ZINC000000006157/ Epinastine		-8.3	Antiallergic
ZINC000000002070/ Sorbinil		-8.3	Inhibitor of aldose reductase
ZINC000000537791/ Glimepiride		-8.2	Antidiabetics

Table 1. (Continued.)

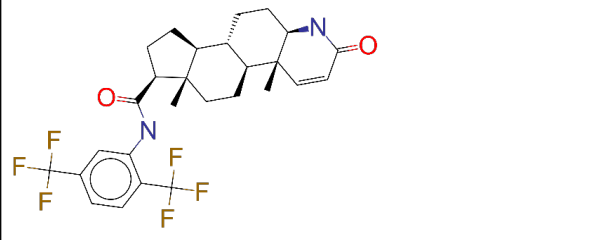
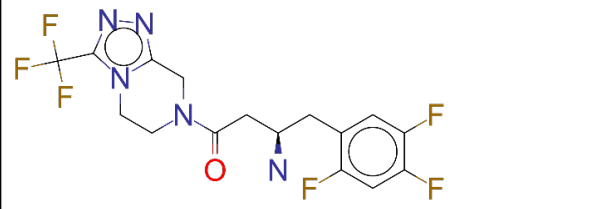
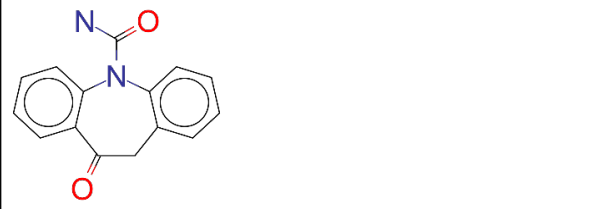
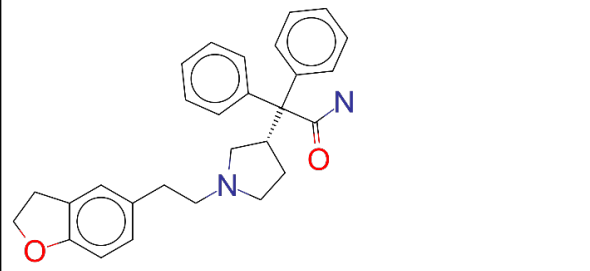
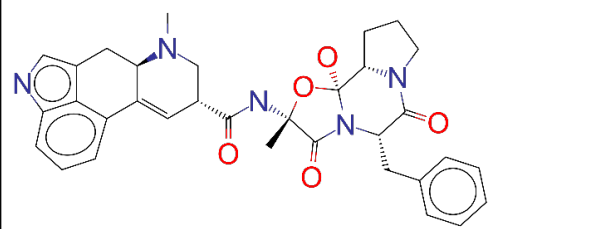
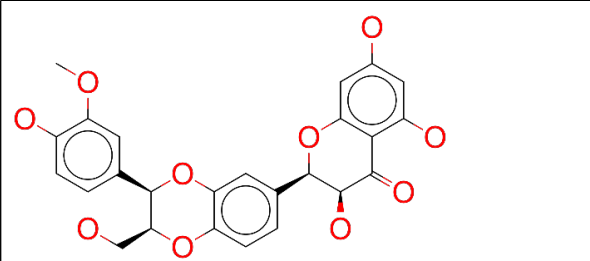
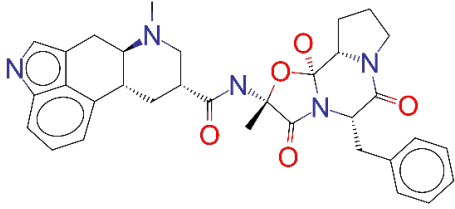
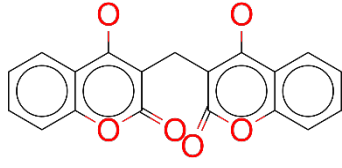
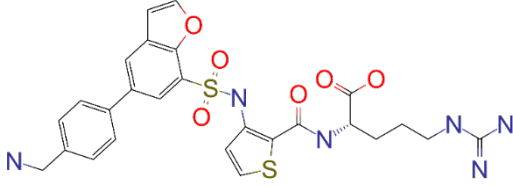
ZINC ID and/or drug name	2D Structure	Vina binding affinity (kcal/mol)	Type
ZINC000003932831/ Dutasteride		-8.2	Antiandrogen
ZINC000001489478/ Sitagliptin		-8.2	Antidiabetics
ZINC000000004724/ Trileptal		-8.2	Antiepileptic
ZINC000001996117/ Darifenacin		-8.1	Treats urinary incontinence
ZINC000052955754/ Ergotamine		-8.1	Antimigraine
ZINC000003831448/ Silibinin		-8.1	Anticancer and various pharmacological effect

Table 1. (Continued.)

ZINC ID and/or drug name	2D Structure	Vina binding affinity (kcal/mol)	Type
ZINC000003978005/ Dihydroergotamine		-8.0	Antimigraine
ZINC000003869855/ Dicumarol		-8.0	Anticoagulant
EG01377		-6.0	Inhibitor of NRP1

pattern of EG01377 in the crystal showed that it can generate hydrogen bond, or interact via van der Waals or pi interactions with Asp³²⁰, Ile⁴¹⁵, Thr³¹⁶, Gly⁴¹⁴, Tyr³⁵³, Lys³⁵¹, Ser³⁴⁶, Thr³⁴⁹, Tyr²⁹⁷, Ser²⁹⁸, Trp³⁰¹, Glu³⁴⁸, and Asn³⁰⁰ (Figure 2B). Among those, hydrogen bond and pi interactions between the inhibitor and Tyr²⁹⁷, Tyr³⁵³, and Trp³⁰¹; and van der Waals interactions generated through Ser²⁹⁸, Ser³⁴⁶, Thr³¹⁶, Ile⁴¹⁵, Gly⁴¹⁴, Thr³⁴⁹, Lys³⁵¹, and Asn³⁰⁰ were reproduced in docking pose as well. However, some hydrogen bond and pi interactions between the inhibitor and amino acids such as inhibitor-Asp³²⁰ and Glu³⁴⁸ in the crystal could not be observed in the docking pose. Hydrogen bond interactions between the inhibitor and Ser²⁹⁸, Thr³⁴⁹, Ser³⁴⁶ in the crystal were generated as van der Waals type interaction in docking conformation (Figure 2C). Note that to compare docking position of EG01377 with that of in crystal, structure with 6FMF PDB ID was used since the binding mode of inhibitor in 6FMF was stated as free of artifact in the original study (Powell et al., 2018). To solidify the idea of using NRP1 inhibitor as an antiviral drug, the binding mode of S protein to NRP1 was analyzed (Daly et al., 2020) and compared with that of EG01377. The peptide of S protein interacts with Asp³²⁰, Tyr²⁹⁷, Trp³⁰¹, Thr³⁴⁹, Lys³⁵¹, Tyr³⁵³, and Ser³⁴⁶ of NRP1 via either of hydrogen bond, pi, and van der Waals interactions. Interaction between EG01377 and all of these amino acids shows that NRP1 inhibitor has the potential to be an antiviral drug. Furthermore, the binding poses of

selected drugs occupy the pocket surrounded by Tyr²⁹⁷, Trp³⁰¹, Lys³⁵¹, and Tyr³⁵³ in docking simulations which supports the idea of these drugs may behave as NRP1 inhibitors (Figures 2D and 2E). To evaluate the persistency and strength of drug-NRP1 complexes near physiological conditions, MD simulations were run.

3.2. MD simulations and binding free energy calculation

In short MD simulations (20 ns) eltrombopag, glimepiride, dutasteride, sitagliptin, and ergotamine stably interacted with NRP1, however, atovaquone and mefloquine did not. These two antimalarial drugs left their initial docking positions and moved to the solution even in two independent trials. Then we extended 20 ns simulations for those who could interact with the protein in these short simulations to 100 ns to assess the stability of their interaction with NRP1. In a control simulation, the EG01377-NRP1 complex obtained from crystal (6FMF) was simulated for 100 ns. Visual inspection of long simulations showed that all selected drugs and the inhibitor retained their docking positions on the NRP1 through the entire simulation. Root mean square deviation analysis (RMSD) of C_α atoms showed that simulations reached equilibrium around 2 Å after an initial jump within 1–2 ns (Figure 3).

To examine the interaction between drugs and critical residues, the contact frequency between drugs and selected amino acids around the binding pocket were visualized. Thus, the persistency of drug-amino

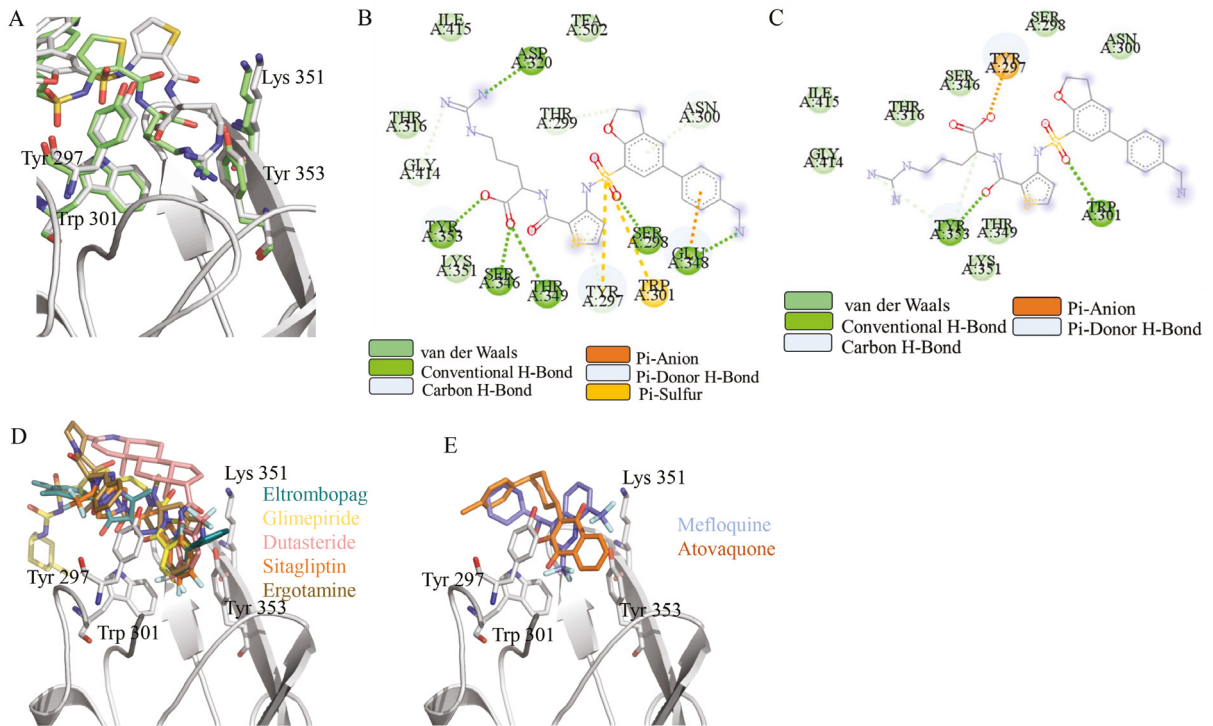


Figure 2. (A) Binding of EG01377 (shown in sticks representation) in the crystal (PDB ID: 6FMF) (carbon atoms are shown in green) in the docking simulation (carbon atoms are shown in white) to b1 domain of NRP1 (shown in white cartoon representation). (B) 2D interaction diagram of EG01377 binding to NRP1 in crystal structure (6FMF). (C) 2D interaction diagram of EG01377 in docking simulation. Diagrams were generated by using Discovery Studio Visualizer. (D) Binding mode of eltrombopag, glimepiride, dutasteride, sitagliptin, and ergotamine to NRP1 obtained from the docking. (E) Binding of two antimalarial drugs mefloquine and atovaquone to NRP1 obtained from the docking.

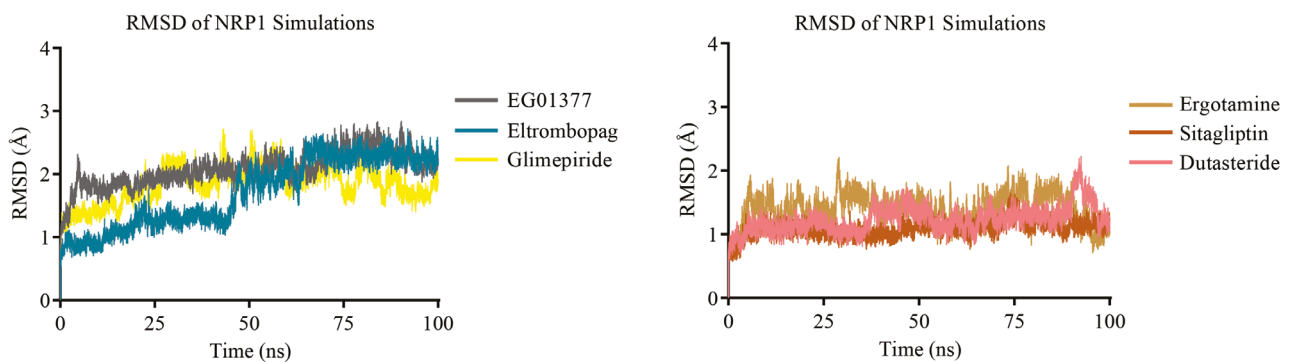


Figure 3. Root mean square deviation (RMSD) of C_α atoms in drug-NRP1 simulations.

acid interactions observed in the initial docking position could be assessed (Figures 4A–4F). Docking of EG01377 showed that the inhibitor interacts with Tyr²⁹⁷, Trp³⁰¹, Thr³¹⁶, Glu³⁴⁸, Thr³⁴⁹, Lys³⁵¹, Tyr³⁵³. In MD simulations, EG01377 interacted frequently with Tyr²⁹⁷, Trp³⁰¹, Thr³¹⁶, and Tyr³⁵³ which have aromatic (Tyr and Trp) and polar (Thr) side chains. In addition to these highly interacting amino acids, the inhibitor interacted with Glu³⁴⁸ and Thr³⁴⁹

through 100 ns simulation (Figure 4A). As a result, MD simulation of EG01377-NRP1 analysis verified interacting residues in the docking. Contact frequency analysis for eltrombopag-NRP1 simulation indicated that similar to EG01377, Tyr²⁹⁷, Trp³⁰¹, Thr³¹⁶, and Tyr³⁵³ are the frequently interacting residues. The same residues were also identified in docking simulation (Figure 4B). In addition to these highly interacting amino acids, interaction between Asp³²⁰

and eltrombopag that is identified in the EG01377-NRP1 crystal structure (6FMF) makes eltrombopag drug a prime candidate. One minor difference between EG01377 and eltrombopag simulations is that while EG01377 interacted with Gly³¹⁸, eltrombopag interacted more with Gly⁴¹⁴.

Glimepiride and sitagliptin frequently interacted with the same amino acids that are Tyr²⁹⁷, Trp³⁰¹, Thr³¹⁶, Thr³⁴⁹, and Tyr³⁵³ (Figures 4C and 4E) in MD simulations. To note some interactions altered throughout the simulations. For example, interaction with highly interacting amino acids Thr³⁴⁹ and Lys³⁵¹ fluctuated as simulations progressed. Despite slight differences in their docking positions, interacting residues in docking simulations are very similar. While glimepiride interacted with Tyr²⁹⁷, Trp³⁰¹, Thr³¹⁶, Glu³⁴⁸, Thr³⁴⁹, and Tyr³⁵³, sitagliptin fitted a deeper part of the pocket and, in addition to glimepiride's interacting amino acids, interacted with Thr³¹⁶ (Figures 4C and 4E). Overall, nearby residues observed in docking simulations of glimepiride and sitagliptin were verified by MD simulations.

The docking position of dutasteride showed that the drug interacts with Tyr²⁹⁷, Thr³⁴⁹, Lys³⁵¹, and Tyr³⁵³. MD

simulation of dutasteride-NRP1 showed that dutasteride behaved less similarly with the inhibitor and did not interact with Trp³⁰¹ and Tyr³⁵³ after a certain time (Figure 4D). Possibly dutasteride translated in the binding pocket and started to interact with new residues such as Gly³¹⁸, Glu³¹⁹, Asp³²⁰, and Ile⁴¹⁵.

Ergotamine showed similar interaction frequency patterns with the inhibitor and constantly interacted with Tyr²⁹⁷, Trp³⁰¹, Thr³¹⁶, and Tyr³⁵³ (Figure 4F). In addition to these, ergotamine interacted with Asp³²⁰, Thr³⁴⁹, and Ile⁴¹⁵ in certain periods of the MD simulation. In docking simulation ergotamine interacted with Tyr²⁹⁷, Trp³⁰¹, Thr³¹⁶, Ser³⁴⁶, Glu³⁴⁸, Thr³⁴⁹, Lys³⁵¹, and Tyr³⁵³. While some of the amino acids recognized in the docking lost contact with ergotamine such as Ser³⁴⁶ and Glu³⁴⁸, most of them interacted with ergotamine in the whole MD simulation.

To determine the binding free energy (BFE) between drugs and NRP1 MM/GBSA method was used. The BFE of eltrombopag, glimepiride, dutasteride, sitagliptin, and ergotamine was calculated as -17.11, -12.55, -9.47, -13.34, and -14.95 kcal/mol, respectively (Table 2). BFE of EG01377 was calculated as -16.19 kcal/mol.

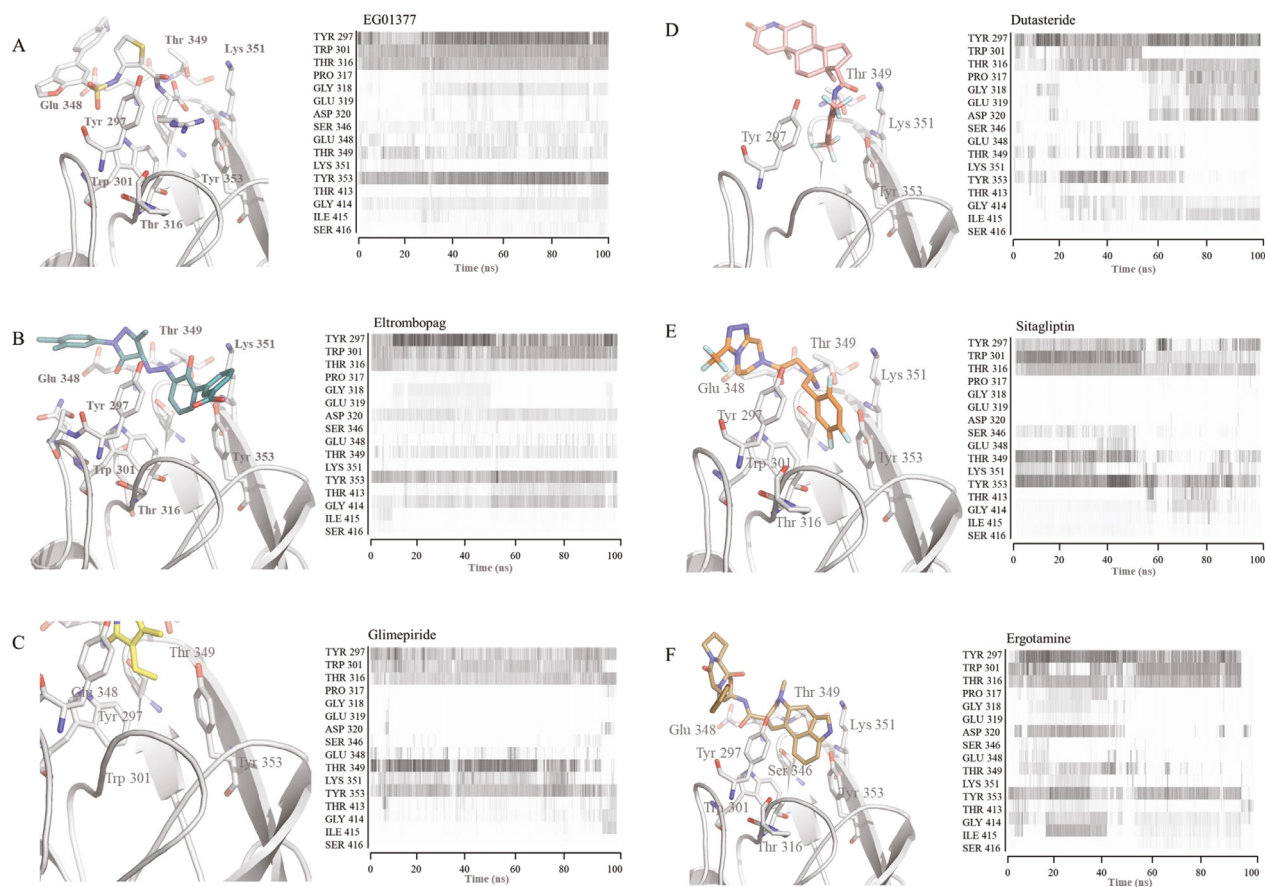


Figure 4. The binding pose in docking simulations and interaction frequency of amino acids from 100 ns MD simulations for NRP1 in complex with (A) EG01377, (B) eltrombopag, (C) glimepiride, (D) dutasteride, (E) sitagliptin, (F) ergotamine.

Table 2. MM/GBSA BFE of selected drugs and NRP1 inhibitor.

Drug name	MM/GBSA BFE (kcal/mol)
Eltrombopag	-17.11 ± 2.99
Ergotamine	-14.95 ± 7.40
Sitagliptin	-13.34 ± 3.90
Glimepiride	-12.55 ± 3.48
Dutasteride	-9.47 ± 4.41
EG01377	-16.19 ± 4.20

A well-tolerated drug eltrombopag stimulates platelet synthesis in patients having low blood platelet (Erickson-Miller et al., 2009). In comparison to EG01377, eltrombopag has comparable Vina binding energy (-8.5 kcal/mol) and BFE (-17.11 kcal/mol) calculated from docking and MD simulations, respectively. During the MD simulations interacting residues of EG01377 and eltrombopag with NRP1 are very similar to each other (Figure 4B). A previous drug-repurposing study against 3CL^{pro} and RdRp of SARS-CoV-2 from our group showed that eltrombopag may bind to the active site of 3CL^{pro} and nsp8 binding site of RdRp which may attenuate the virus activity (Gul et al., 2020). Eltrombopag exhibits in vitro antiviral properties with IC₅₀ lower than 10µM (Jeon et al., 2020). This report shows that eltrombopag can strongly interact with NRP1, as well. If these in silico findings can be verified by in vitro and cell-culture experiments, eltrombopag can be a very strong antiviral drug by blocking SARS-CoV-2-NRP1 binding to host and alleviating the virus replication.

Two antidiabetics, glimepiride and sitagliptin are well-tolerated drugs used to treat type2 diabetes (Bautista et al., 2003; Raz et al., 2008). Both drugs have the same Vina binding energies (-8.2 kcal) in docking simulations and very similar BFEs calculated from MM/GBSA analysis that are -13.34 and -12.55 kcal/mol for sitagliptin and glimepiride, respectively. Interacting amino acid residues and BFEs of these antidiabetics are quite alike to EG01377 (Figures 4C and 4E). Sitagliptin is an inhibitor of dipeptidyl-peptidase IV (DPP-4) that is the host receptor of the Middle East respiratory syndrome (MERS)-CoV (Karasik et al., 2008; Raj et al., 2013) and in silico studies suggested that protein S of SARS-CoV-2 can bind to DPP4 as well (Li et al., 2020b; Vankadari and Wilce, 2020). Administration of sitagliptin to patients suffering from diabetes and COVID-19 does not only help to lower the blood glucose level but may also reduce the SARS-CoV-2 entry to the cells.

Dutasteride, another well-tolerated drug, inhibits type I and II 5α-reductase and shows antiandrogenic activity (Roehrborn et al., 2002; Andriole and Kirby, 2003).

5α-reductase converts testosterone to dihydrotestosterone and enlarges the prostate glands. Thus, dutasteride is used to treat prostatic conditions by blocking the 5α-reductase activity (Makridakis et al., 2000). Besides the effect on the prostate gland, dutasteride suppresses the transmembrane serine protease 2 (TMPRSS2) expression (Mostaghel et al., 2014) which primes protein S of the SARS-CoV-2 (Hoffmann et al., 2020b). Docking binding energy and MM/GBSA calculations show that dutasteride has a high affinity to NRP1 (Tables 1 and 2). Relatively higher BFE with a high standard deviation of dutasteride-NRP1 may stem from the loss of interaction between dutasteride and two aromatic residues Trp³⁰¹ and Tyr³⁵³ as shown in contact frequency analysis (Figure 4D). However, dutasteride has still a high affinity to the NRP1 and interacts with amino acids observed in docking simulations. Despite further in vivo analysis needed, dutasteride may be a preventive drug that shuts down the virus entry by blocking the NRP1 and downregulating the TMPRSS2.

Antimigraine ergotamine is a tolerable drug with mild and transient side effects (Diener et al., 2002; Christie et al., 2003). Several in silico drug repurposing studies reported that ergotamine may inhibit the RdRp and 3CL^{pro} of SARS-CoV-2 (Barage et al., 2020; Gul et al., 2020). Ergotamine has the second-best BFE among all drugs analyzed in this study (Table 2). Comparable BFEs of ergotamine and EG01377 to NRP1 suggests that ergotamine can strongly bind to NRP1, in turn, can attenuate NRP1-protein S binding. If these computational analyses can be experimentally verified, ergotamine can be used to mitigate the COVID-19. To note, it has been reported that ergotamine may cross-react with antiviral drugs (Rosenthal et al., 1999; Mortier et al., 2001; Ayarragaray, 2014). Thus, further studies related to ergotamine should be designed accordingly.

Comparable BFE and interaction pattern of inhibitor and selected drugs indicate that these drugs may act as NRP1 inhibitors.

3.3. H-bond and Alanine scanning analysis

To determine the number of hydrogen bonds drug made during the MD simulation, the hydrogen bond (H-bond) generated by drugs to any amino acids through 100 ns were analyzed (Figure 5). Calculation of the average number of H-bonds showed that each drug, including the inhibitor, produced less than one H-bond per frame. Interaction types between selected drugs and protein were analyzed and represented in a two-dimensional diagram (Figure 6). Analyses showed that the inhibitor and all drugs interact with the protein through hydrophobic interactions, and conduct hydrogen bond and at least one type of pi interaction. Since drugs of interest possess aromatic rings, charged or aromatic amino acids on NRP1 generate those interactions. Tyr²⁹⁷ consistently generated pi interactions,

Trp³⁰¹ and Tyr³⁵³ have generated either H-bond or pi interactions with all drugs. Ser²⁹⁸, Thr³¹⁶, Glu³⁴⁸, and Gly⁴¹⁴ interacted with drugs through van der Waals interactions and generated hydrophobic interactions. Ser²⁹⁸ formed hydrogen bonds only with EG01377 and ergotamine. Glu³⁴⁸ generated pi interactions and hydrogen bonds with EG01377 and glimepiride, and only pi interactions with eltrombopag.

Despite drugs suggested to behave like NRP1 inhibitor have diverse structures, they have some common properties. For example, all drugs analyzed in details have multiple ring structures at least one with aromatic. Second, all these organic compounds bear polar groups such as carbonyl group or halogen atoms that have ability to generate hydrogen bonds or pi interactions with amino acids. Third, drugs have 70 to 110 atoms in their structure that allow them to generate high number of van der Waals interaction with the protein. These common properties of drugs cause tight binding to NRP1.

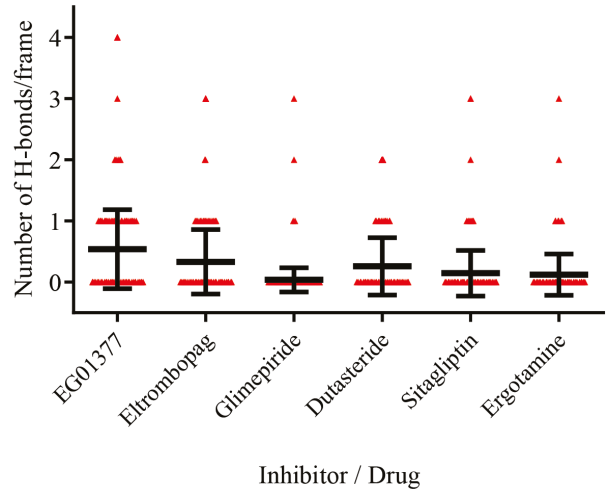


Figure 5. H-bond analysis of each drug/inhibitor made to NRP1 (per frame) in MD simulation. A total of 25,000 frames (every 4ps) were included for this calculation.

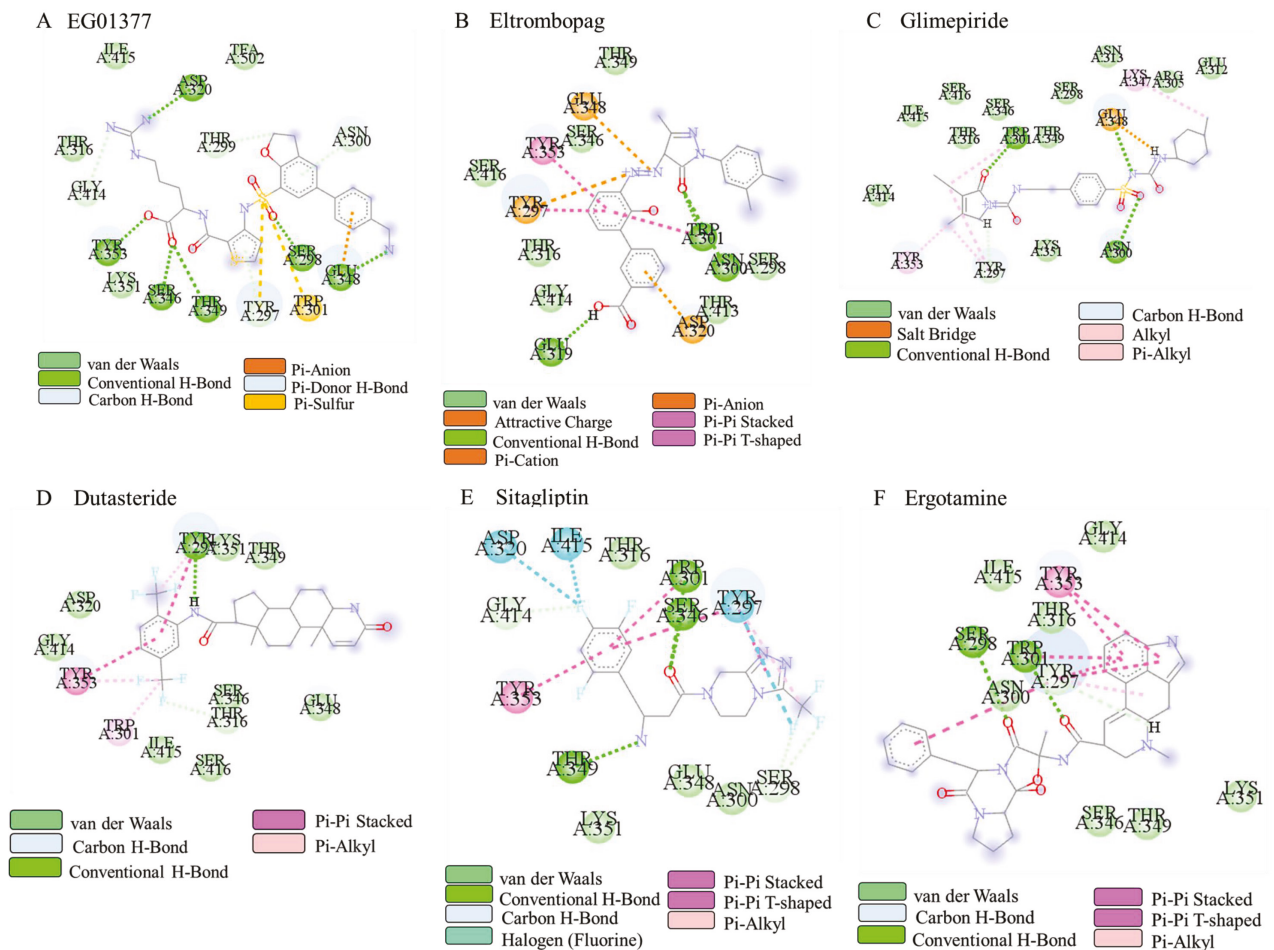


Figure 6. Two-dimensional diagram of interaction type between NRP1 in complex with (A) EG01377 in crystal structure (6FMF), or (B) eltrombopag, (C) glimepiride, (D) dutasteride, (E) sitagliptin, (F) ergotamine obtained from docking simulations.

To reveal the critical amino acids for drug binding and quantify their contribution to BFE, *in silico* Alanine scanning mutation was performed. The most frequently and commonly interacting amino acids e.g., Tyr²⁹⁷, Trp³⁰¹, Thr³¹⁶, and Tyr³⁵³ in all drug/inhibitor-NRP1 simulations were analyzed (Figures 4A–4F). These residues were mutated to Alanine one by one and BFE between drugs and NRP1 was calculated using the MM/GBSA method (Table 3). Then the difference between BFEs of drugs against mutant and wild-type NRP1 is calculated ($\Delta\Delta G$). $\Delta\Delta G$ values larger than 0 means that mutation is destabilizing the interaction, $\Delta\Delta G$ lower than 0 means mutation is stabilizing the interaction. Free energy change in protein-protein interaction at equilibrium is calculated by using the following formula: $\Delta G^\circ = -RT \ln K_{eq}$ where ΔG° is the standard free energy change, R is the gas constant, T is the absolute temperature. Using $R = 1.987 \times 10^{-3}$ kcal/mol, $T = 298$ K in that formula gives that increase in 0.4–0.5 kcal/mol in ΔG° ($\Delta\Delta G$ in our data), leads to 2-fold decrease in ligand bound protein state. Thus, mutations causing $\Delta\Delta G > 0.5$ kcal/mol were evaluated as critical amino acid for drug-protein binding. According to $\Delta\Delta G$ values, Tyr²⁹⁷, Trp³⁰¹, and Tyr³⁵³ are very critical for all drugs binding to NRP1. Interestingly, despite high interaction with drugs, Thr³¹⁶ minimally contributes to BFE. Tyr²⁹⁷ has the highest contribution to BFE, -4.03, -4.12, -2.24 kcal/mol, in NRP1-EG01377, eltrombopag, and dutasteride simulations, respectively. Trp³⁰¹ is the second highest contributor to BFE in EG01377 (-3.1 kcal/mol), eltrombopag (-2.36 kcal/mol), and sitagliptin (-2.60 kcal/mol) simulations and top contributor to BFE in ergotamine-NRP1 simulation (-2.43 kcal/mol). Tyr³⁵³ has a similar effect on the binding of eltrombopag to NRP1 with Trp³⁰¹ and contributes -2.37 kcal/mol to BFE. Tyr³⁵³ has also the highest effect on BFE in sitagliptin (-3.06 kcal/mol) and glimepiride (-2.39 kcal/mol) simulations. (Table 3). The contribution of each mutated amino acid to drug-NRP1 BFE is given (Figure 7).

H-bond and Alanine scanning calculations provide a deeper understanding of drug-NRP1 interactions. Future structure-activity relationship (SAR) studies aim to design a more potent NRP1 inhibitor may benefit from the critical amino acids identified here. Adding an H-bond donor or acceptor to a new molecule can increase the binding affinity to NRP1.

4. Conclusion

Despite substantial progress has been made by several companies for the SARS-CoV-2 vaccine (Corbett et al., 2020; Mulligan et al., 2020; Sahin et al., 2020) only several governments approved for emergency use authorization. Therefore, medication is still an essential element to combat COVID-19. Vital enzymes of SARS-CoV-2 such as proteases (3CL^{pro} and M^{pro}) and RNA polymerase (RdRp), or virus binding receptors on the host such as ACE2 or TMPRSS2 are generally targeted in drug repurposing studies (Bagheri and Niavarani, 2020; Busnadiego et al., 2020; Carino et al., 2020; Gul et al., 2020; Kumar et al., 2020; Li et al., 2020c; Singh et al., 2020b). Recent studies reported protein S binds to NRP1 which facilitates SARS-CoV-2 host entry (Cantuti-Castelvetri et al., 2020; Daly et al., 2020). Here a drug repurposing study was done against NRP1 in terms of docking and MD simulations using the FDA approved drugs. Furthermore, key amino acids on NRP1 for drug binding were identified by running Alanine scanning analysis. Several well-tolerated drugs showed comparable and even better affinity to NRP1 than its inhibitor EG01377. Eltrombopag had the best binding affinity to NRP1 among all drugs. In addition to eltrombopag, two antidiabetics, sitagliptin and glimepiride stably interacted with and exhibited high affinity to NRP1. Since patients having chronic diseases such as diabetes are at more risk against COVID-19, those suffering from diabetes may benefit from sitagliptin and glimepiride not only as antidiabetics but also their preventive effects, if proven by experiment, against SARS-CoV-2 infection.

Table 3. MM/GBSA BFE after Alanine mutations of selected residues.

Mutations Drugs	BFE (kcal/mol)			
	Y297A/ $\Delta\Delta G$	W301A/ $\Delta\Delta G$	T316A/ $\Delta\Delta G$	Y353A/ $\Delta\Delta G$
Eltrombopag	-12.99/4.12	-14.75/2.36	-16.65/0.46	-14.74/2.37
Ergotamine	-12.77/2.18	-12.52/2.43	-14.63/0.32	-13.41/1.54
Sitagliptin	-11.56/1.78	-10.74/2.60	-12.79/0.55	-10.28/3.06
Glimepiride	-11.27/1.28	-11.51/1.04	-12.65/-0.10	-10.16/ 2.39
Dutasteride	-7.23/2.24	-8.84/0.63	-9.23/0.24	-8.72/0.75
EG01377	-12.16/4.03	-13.09/3.1	-15.44/0.75	-14.03/2.16

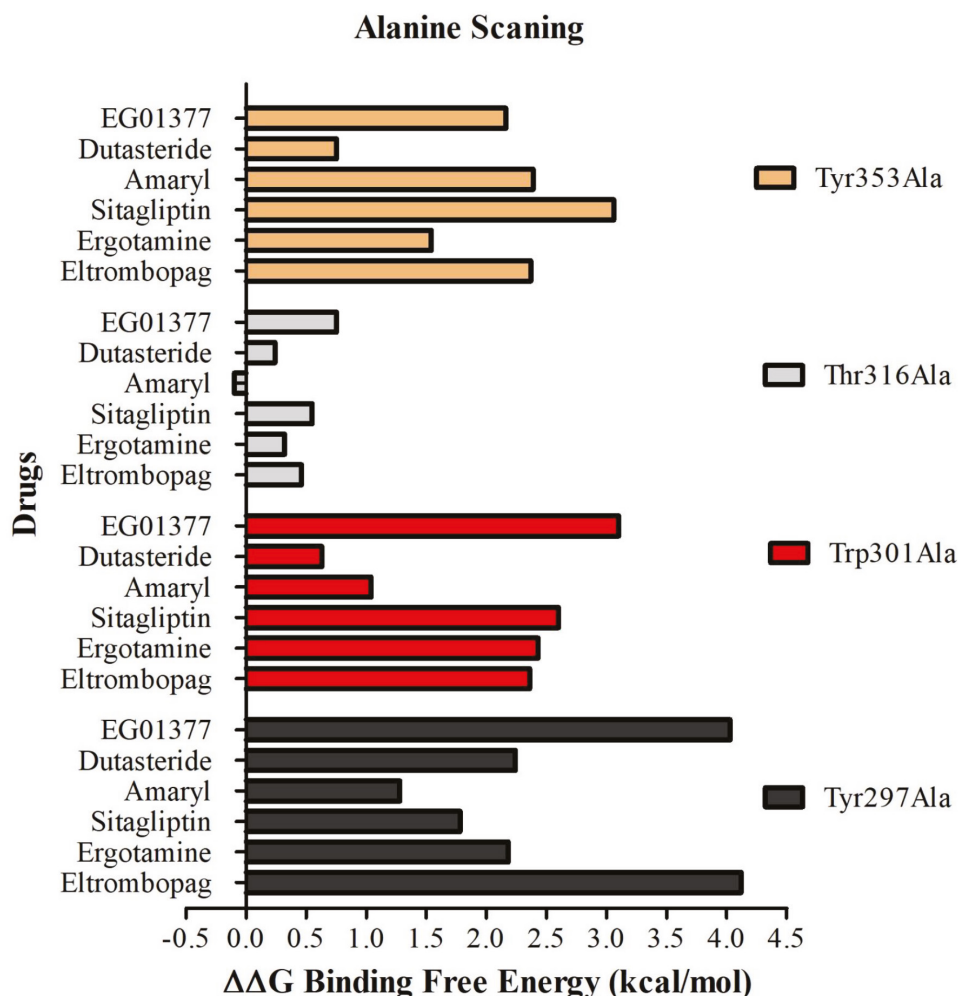


Figure 7. Contribution of critical residues to BFE in drug-NRP1 binding.

Dutasteride may provide multiple benefits to COVID-19 patients. First, it reduces the expression of TMPRSS2 that primes the S-protein (Hoffmann et al., 2020a; Hoffmann et al., 2020b). Second, in silico studies reported that it may block 3CL^{pro} (Gul et al., 2020). Third, this study shows that dutasteride can bind to and strongly interact with NRP1, thus, may decrease SARS-CoV-2 entry. Ergotamine is another top candidate molecule for the NRP1 binding. Previous calculations showed that ergotamine has the potential to bind to 3CL^{pro} and RdRp of SARS-CoV-2 (Gul et al., 2020; Rahman et al., 2020). Therefore, ergotamine may inhibit SARS-CoV-2 at the infection and replication stages. Alanine scanning calculations uncovered that Tyr²⁹⁷, Trp³⁰¹, and Tyr³⁵³ are the most critical amino acid residues for drug binding to NRP1. H-bond analysis and Alanine scanning results may be exploited by further inhibitor design studies.

To expedite the discovery of therapeutics for COVID-19 drug repurposing studies may provide a rational starting point. If the findings of this study can be verified by in vitro, in vivo, and clinical trials these well-tolerated and cost-effective drugs can be adapted to current protocols used to treat COVID-19.

Acknowledgment/disclaimer/conflict of interest

I would like to thank to Dr. İ. Halil Kavaklı from Koç University for his critical reading of the manuscript.

The numerical calculations reported in this paper were partially performed at TÜBİTAK ULAKBİM, High Performance and Grid Computing Center (TRUBA resources).

The author declares no conflict of interest.

References

- Andriole GL, Kirby R (2003). Safety and tolerability of the dual 5 alpha-reductase inhibitor dutasteride in the treatment of benign prostatic hyperplasia. *European Urology* 44 (1): 82-88. doi: 10.1016/S0302-2838(03)00198-2
- Ayarragaray JE (2014). Ergotism: a change of perspective. *Annals of Vascular Surgery* 28 (1): 265-268. doi: 10.1016/j.avsg.2013.02.005
- Baez-Santos YM, St John SE, Mesecar AD (2015). The SARS-coronavirus papain-like protease: structure, function and inhibition by designed antiviral compounds. *Antiviral Research* 115: 21-38. doi: 10.1016/j.antiviral.2014.12.015
- Bagheri M, Niavarani A (2020). Molecular dynamics analysis predicts ritonavir and naloxegol strongly block the SARS-CoV-2 spike protein-hACE2 binding. *Journal of Biomolecular Structure & Dynamics* 1-10. doi: 10.1080/07391102.2020.1830854
- Barage S, Karthic A, Bavi R, Desai N, Kumar R et al. (2020). Identification and characterization of novel RdRp and Nsp15 inhibitors for SARS-COV2 using computational approach. *Journal of Biomolecular Structure & Dynamics* 1-18. doi: 10.1080/07391102.2020.1841026
- Bautista JL, Bugos C, Dirnberger G, Atherton T (2003). Efficacy and safety profile of glimepiride in Mexican American patients with type 2 diabetes mellitus: A randomized, placebo-controlled study. *Clinical Therapeutics* 25 (1): 194-209. doi: 10.1016/S0149-2918(03)90025-7
- Bharadwaj S, Azhar EI, Kamal MA, Bajrai LH, Dubey A et al. (2020). SARS-CoV-2 M-pro inhibitors: identification of anti-SARS-CoV-2 M-pro compounds from FDA approved drugs. *Journal of Biomolecular Structure & Dynamics* doi: 10.1080/07391102.2020.1842807
- Boopathi S, Poma AB, Kolandaivel P (2020). Novel 2019 coronavirus structure, mechanism of action, antiviral drug promises and rule out against its treatment. *Journal of Biomolecular Structure & Dynamics* doi: 10.1080/07391102.2020.1758788
- Busnadiego I, Fernbach S, Pohl MO, Karakus U, Huber M et al. (2020). Antiviral activity of type I, II, and III interferons counterbalances ACE2 inducibility and restricts SARS-CoV-2. *Mbio* 11 (5). doi: 10.1128/mBio.01928-20
- Cantuti-Castelvetri L, Ojha R, Pedro LD, Djannatian M, Franz J et al. (2020). Neuropilin-1 facilitates SARS-CoV-2 cell entry and infectivity. *Science* 370 (6518): 856-860. doi: 10.1126/science.abd2985
- Cao S, Yaqoob U, Das A, Shergill U, Jagavelu K et al. (2010). Neuropilin-1 promotes cirrhosis of the rodent and human liver by enhancing PDGF/TGF-beta signaling in hepatic stellate cells. *Journal of Clinical Investigation* 120 (7): 2379-2394. doi: 10.1172/JCI41203
- Carino A, Moraca F, Fiorillo B, Marchiano S, Sepe V et al. (2020). Hijacking SARS-CoV-2/ACE2 receptor interaction by natural and semi-synthetic steroidal agents acting on functional pockets on the receptor binding domain. *Frontiers in Chemistry* 8: 572885. doi: 10.3389/fchem.2020.572885
- Case DA, Cheatham III TE, Darden T, Gohlke H, Luo R et al. (2005). The Amber biomolecular simulation programs. *Journal of Computational Chemistry* 26 (16): 1668-1688. doi: 10.1002/jcc.20290
- Choudhary S, Malik Y S, Tomar S (2020). Identification of SARS-CoV-2 cell entry inhibitors by drug repurposing using in silico structure-based virtual screening approach. *Frontiers in Immunology* 11. doi: 10.3389/fimmu.2020.01664
- Christie S, Gobel H, Mateos V, Allen C, Vrijens F et al. (2003). Crossover comparison of efficacy and preference for rizatriptan 10 mg versus ergotamine/caffeine in migraine. *European Neurology* 49 (1): 20-29. doi: 10.1159/000067018
- Corbett KS, Flynn B, Foulds KE, Francica JR, Boyoglu-Barnum S et al. (2020). Evaluation of the mRNA-1273 vaccine against SARS-CoV-2 in nonhuman primates. *New England Journal of Medicine* 383 (16): 1544-1555. doi: 10.1056/NEJMoa2024671
- Daly JL, Simonetti B, Klein K, Chen KE, Williamson MK et al. (2020). Neuropilin-1 is a host factor for SARS-CoV-2 infection. *Science* 370 (6518): 861-865. doi: 10.1126/science.abd3072
- DeLano WL (2009). PyMOL molecular viewer: updates and refinements. *Abstracts of Papers of the American Chemical Society* 238.
- Diener HC, Jansen JP, Reches A, Pascual J, Pitei D et al. (2002). Efficacy, tolerability and safety of oral eletriptan and ergotamine plus caffeine (Cafergot (R)) in the acute treatment of migraine: a multicentre, randomised, double-blind, placebo-controlled comparison. *European Neurology* 47 (2): 99-107. doi: 10.1159/000047960
- Donoghue M, Hsieh F, Baronas E, Godbout K, Gosselin M et al. (2000). A novel angiotensin-converting enzyme-related carboxypeptidase (ACE2) converts angiotensin I to angiotensin 1-9. *Circulation Research* 87 (5): E1-E9. doi: 10.1161/01.res.87.5.e1
- Doruk YU, Yarpurvar D, Akyel YK, Gul S, Taskin AC et al. (2020). A CLOCK-binding small molecule disrupts the interaction between CLOCK and BMAL1 and enhances circadian rhythm amplitude. *Journal of Biological Chemistry* 295 (11): 3518-3531. doi: 10.1074/jbc.RA119.011332
- Du QS, Wang SQ, Zhu Y, Wei DQ, Guo H et al. (2004). Polyprotein cleavage mechanism of SARS CoV M-pro and chemical modification of the octapeptide. *Peptides* 25 (11): 1857-1864. doi: 10.1016/j.peptides.2004.06.018
- Durdađı S (2020). Virtual drug repurposing study against SARS-CoV-2 TMPRSS2 target. *Turkish Journal of Biology* 44 (3): 185-191. doi: 10.3906/biy-2005-112.
- Erickson-Miller CL, Delorme E, Tian SS, Hopson CB, Landis AJ et al. (2009). Preclinical activity of eltrombopag (SB-497115), an oral, nonpeptide thrombopoietin receptor agonist. *Stem Cells* 27 (2): 424-430. doi: 10.1634/stemcells.2008-0366

- Fantin A, Herzog B, Mahmoud M, Yamaji M, Plein A et al. (2014). Neuropilin 1 (NRP1) hypomorphism combined with defective VEGF-A binding reveals novel roles for NRP1 in developmental and pathological angiogenesis. *Development* 141 (3): 556-562. doi: 10.1242/dev.103028
- Ghosh R, Chakraborty A, Biswas A, Chowdhuri S (2020). Potential therapeutic use of corticosteroids as SARS-CoV-2 main protease inhibitors: a computational study. *Journal of Biomolecular Structure & Dynamics*. doi: 10.1080/07391102.2020.1835728
- Gul S, Ozcan O, Asar S, Okyar A, Baris I et al. (2020). In silico identification of widely used and well-tolerated drugs as potential SARS-CoV-2 3C-like protease and viral RNA-dependent RNA polymerase inhibitors for direct use in clinical trials. *Journal of Biomolecular Structure & Dynamics*. doi: 10.1080/07391102.2020.1802346
- Hoffmann M, Kleine-Weber H, Pohlmann S (2020a). A multibasic cleavage site in the spike protein of SARS-CoV-2 is essential for infection of human lung cells. *Molecular Cell* 78 (4): 779-784 e775. doi:10.1016/j.molcel.2020.04.022
- Hoffmann M, Kleine-Weber H, Schroeder S, Kruger N, Herrler T et al. (2020b). SARS-CoV-2 cell entry depends on ACE2 and TMPRSS2 and is blocked by a clinically proven protease inhibitor. *Cell* 181 (2): 271-280 e278. doi: 10.1016/j.cell.2020.02.052
- Huang J, Rauscher S, Nawrocki G, Ran T, Feig M et al. (2017). CHARMM36m: an improved force field for folded and intrinsically disordered proteins. *Nature Methods* 14 (1): 71-73. doi: 10.1038/Nmeth.4067
- Humphrey W, Dalke A, Schulten K (1996). VMD: Visual molecular dynamics. *Journal of Molecular Graphics & Modelling* 14 (1): 33-38. doi: 10.1016/0263-7855(96)00018-5
- Jarvis A, Allerston CK, Jia H, Herzog B, Garza-Garcia A et al. (2010). Small molecule inhibitors of the neuropilin-1 vascular endothelial growth factor A (VEGF-A) interaction. *Journal of Medicinal Chemistry* 53 (5): 2215-2226. doi: 10.1021/jm901755g
- Jeon S, Ko M, Lee J, Choi I, Byun SY et al. (2020). Identification of antiviral drug candidates against SARS-CoV-2 from FDA-approved drugs. *Antimicrobial Agents and Chemotherapy* 64 (7): e00819-00820. doi: 10.1128/AAC.00819-20
- Jia H, Aqil R, Cheng L, Chapman C, Shaikh S et al. (2014). N-terminal modification of VEGF-A C terminus-derived peptides delineates structural features involved in neuropilin-1 binding and functional activity. *Chembiochem* 15 (8): 1161-1170. doi: 10.1002/cbic.201300658
- Jo S, Kim T, Iyer VG, Im W (2008). Software news and updates - CHARNIM-GUI: a web-based graphical user interface for CHARMM. *Journal of Computational Chemistry* 29 (11): 1859-1865. doi: 10.1002/jcc.20945
- Karasik A, Aschner P, Katzeff H, Davies MJ, Stein PP (2008). Sitagliptin, a DPP-4 inhibitor for the treatment of patients with type 2 diabetes: a review of recent clinical trials. *Current Medical Research and Opinion* 24 (2): 489-496. doi: 10.1185/030079908X261069
- Kim S, Lee J, Jo S, Brooks CL, Lee HS et al. (2017). CHARMM-GUI ligand reader and modeler for CHARMM force field generation of small molecules. *Journal of Computational Chemistry* 38 (21): 1879-1886. doi: 10.1002/jcc.24829
- Kumar V, Dhanjal JK, Bhargava P, Kaul A, Wang J et al. (2020). Withanone and Withaferin-A are predicted to interact with transmembrane protease serine 2 (TMPRSS2) and block entry of SARS-CoV-2 into cells. *Journal of Biomolecular Structure & Dynamics* 1-13. doi: 10.1080/07391102.2020.1775704
- Li HO, Zhou YJ, Zhang M, Wang HZ, Zhao Q et al. (2020a). Updated Approaches against SARS-CoV-2. *Antimicrobial Agents and Chemotherapy* 64 (6): e00483-00420. doi: 10.1128/AAC.00483-20
- Li Y, Zhang ZD, Yang L, Lian XY, Xie Y et al. (2020b). The MERS-CoV receptor DPP4 as a candidate binding target of the SARS-CoV-2 spike. *Iscience* 23 (6): 1-15. doi: 10.1016/j.isci.2020.101160
- Li Z, Li X, Huang YY, Wu YX, Liu RD et al. (2020c). Identify potent SARS-CoV-2 main protease inhibitors via accelerated free energy perturbation-based virtual screening of existing drugs. *Proceedings of the National Academy of Sciences of the United States of America* 117 (44): 27381-27387. doi: 10.1073/pnas.2010470117
- Liu Y, Mao B, Liang S, Yang JW, Lu H W et al. (2020). Association between age and clinical characteristics and outcomes of COVID-19. *European Respiratory Journal* 55 (5): 1-4. doi: 10.1183/13993003.01112-2020
- Makridakis NM, Di Salle E, Reichardt JK (2000). Biochemical and pharmacogenetic dissection of human steroid 5 alpha-reductase type II. *Pharmacogenetics* 10 (5): 407-413. doi: 10.1097/00008571-200007000-00004
- Mortier E, Pouchot J, Vinceneux P, Lalande M (2001). Ergotism related to interaction between nelfinavir and ergotamine. *American Journal of Medicine* 110 (7): 594-594. doi: 10.1016/S0002-9343(01)00655-6
- Mostaghel EA, Nelson PS, Lange P, Lin DW, Taplin ME et al. (2014). Targeted androgen pathway suppression in localized prostate cancer: a pilot study. *Journal of Clinical Oncology* 32 (3): 229-237. doi: 10.1200/JCO.2012.48.6431
- Mota F, Fotinou C, Rana RR, Chan AWE, Yelland T et al. (2018). Architecture and hydration of the arginine-binding site of neuropilin-1. *Febs Journal* 285 (7): 1290-1304. doi: 10.1111/febs.14405
- Mulligan MJ, Lyke KE, Kitchin N, Absalon J, Gurtman A et al. (2020). Phase I/II study of COVID-19 RNA vaccine BNT162b1 in adults. *Nature* 586 (7830): 589-593. doi: 10.1038/s41586-020-2639-4
- Muramatsu T, Kim YT, Nishii W, Terada T, Shirouzu M et al. (2013). Autoprocessing mechanism of severe acute respiratory syndrome coronavirus 3C-like protease (SARS-CoV 3CLpro) from its polyproteins. *Febs Journal* 280 (9): 2002-2013. doi: 10.1111/febs.12222

- Omori R, Matsuyama R, Nakata Y (2020). The age distribution of mortality from novel coronavirus disease (COVID-19) suggests no large difference of susceptibility by age. *Scientific Reports* 10 (1): 16642. doi: 10.1038/s41598-020-73777-8
- Parker MW, Xu P, Li X, Vander Kooi CW (2012). Structural basis for selective vascular endothelial growth factor-A (VEGF-A) binding to neuropilin-1. *Journal of Biological Chemistry* 287 (14): 11082-11089. doi: 10.1074/jbc.M111.331140
- Phillips JC, Braun R, Wang W, Gumbart J, Tajkhorshid E et al. (2005). Scalable molecular dynamics with NAMD. *Journal of Computational Chemistry* 26 (16): 1781-1802. doi: 10.1002/jcc.20289
- Powell J, Mota F, Steadman D, Soudy C, Miyauchi JT et al. (2018). Small molecule neuropilin-1 antagonists combine antiangiogenic and antitumor activity with immune modulation through reduction of transforming growth factor beta (TGF beta) production in regulatory T-cells. *Journal of Medicinal Chemistry* 61 (9): 4135-4154. doi: 10.1021/acs.jmedchem.8b00210
- Rahman MM, Saha T, Islam KJ, Suman RH, Biswas S et al. (2020). Virtual screening, molecular dynamics and structure-activity relationship studies to identify potent approved drugs for Covid-19 treatment. *Journal of Biomolecular Structure & Dynamics* 1-11. doi: 10.1080/07391102.2020.1794974
- Raj VS, Mou HH, Smits SL, Dekkers DHW, Muller MA et al. (2013). Dipeptidyl peptidase 4 is a functional receptor for the emerging human coronavirus-EMC. *Nature* 495 (7440): 251-254. doi: 10.1038/nature12005
- Raz I, Chen Y, Wu M, Hussain S, Kaufman KD et al. (2008). Efficacy and safety of sitagliptin added to ongoing metformin therapy in patients with type 2 diabetes. *Current Medical Research and Opinion* 24 (2): 537-550. doi: 10.1185/030079908X260925
- Roehrborn CG, Boyle P, Nickel JC, Hoefner K, Andriole G et al. (2002). Efficacy and safety of a dual inhibitor of 5-alpha-reductase types 1 and 2 (dutasteride) in men with benign prostatic hyperplasia. *Urology* 60 (3): 434-441. doi: 10.1016/s0090-4295(02)01905-2
- Rosenthal E, Sala F, Chichmanian RM, Batt M, Cassuto JP (1999). Ergotism related to concurrent administration of ergotamine tartrate and indinavir. *JAMA* 281 (11): 987. doi: 10.1001/jama.281.11.987
- Sahin U, Muik A, Derhovanessian E, Vogler I, Kranz LM et al. (2020). COVID-19 vaccine BNT162b1 elicits human antibody and T(H)1T cell responses. *Nature* 586 (7830): 594-599. doi: 10.1038/s41586-020-2814-7
- Sarma P, Shekhar N, Prajapat M, Avti P, Kaur H et al. (2021). In-silico homology assisted identification of inhibitor of RNA binding against 2019-nCoV N-protein (N terminal domain). *Journal of Biomolecular Structure & Dynamics* 39 (8): 2724-2732. doi: 10.1080/07391102.2020.1753580
- Schoeman D, Fielding BC (2019). Coronavirus envelope protein: current knowledge. *Virology Journal* 16 (1): 69. doi: 10.1186/s12985-019-1182-0
- Shang J, Wan YS, Luo CM, Ye G, Geng QB et al. (2020). Cell entry mechanisms of SARS-CoV-2. *Proceedings of the National Academy of Sciences of the United States of America* 117 (21): 11727-11734. doi: 10.1073/pnas.2003138117
- Shapovalov MV, Dunbrack Jr RL (2011). A smoothed backbone-dependent rotamer library for proteins derived from adaptive kernel density estimates and regressions. *Structure* 19 (6): 844-858. doi: 10.1016/j.str.2011.03.019
- Singh KK, Chaubey G, Chen JY, Suravajhala P (2020a). Decoding SARS-CoV-2 hijacking of host mitochondria in COVID-19 pathogenesis. *American Journal of Physiology-Cell Physiology* 319 (2): C258-C267. doi: 10.1152/ajpcell.00224.2020
- Singh N, Decroly E, Khatib AM, Villoutreix BO (2020b). Structure-based drug repositioning over the human TMPRSS2 protease domain: search for chemical probes able to repress SARS-CoV-2 Spike protein cleavages. *European Journal of Pharmaceutical Sciences* 153: 105495. doi: 10.1016/j.ejps.2020.105495
- Soker S, Takashima S, Miao HQ, Neufeld G, Klagsbrun M (1998). Neuropilin-1 is expressed by endothelial and tumor cells as an isoform-specific receptor for vascular endothelial growth factor. *Cell* 92 (6): 735-745. doi: 10.1016/S0092-8674(00)81402-6
- Sulpice E, Plouet J, Berge M, Allanic D, Tobelem G et al. (2008). Neuropilin-1 and neuropilin-2 act as coreceptors, potentiating proangiogenic activity. *Blood* 111 (4): 2036-2045. doi: 10.1182/blood-2007-04-084269
- Tardu M, Rahim F, Kavakli I H, Turkay M (2016). Milp-hyperbox classification for structure-based drug design in the discovery of small molecule inhibitors of sirtuin 6. *Rairo-Operations Research* 50 (2): 387-400. doi: 10.1051/ro/2015042
- Teesalu T, Sugahara KN, Kotamraju VR, Ruoslahti E (2009). C-end rule peptides mediate neuropilin-1-dependent cell, vascular, and tissue penetration. *Proceedings of the National Academy of Sciences of the United States of America* 106 (38): 16157-16162. doi: 10.1073/pnas.0908201106
- Thiel V, Ivanov KA, Putics A, Hertzog T, Schelle B et al. (2003). Mechanisms and enzymes involved in SARS coronavirus genome expression. *Journal of General Virology* 84 (Pt 9): 2305-2315. doi: 10.1099/vir.0.19424-0
- Trott O, Olson AJ (2010). AutoDock Vina: improving the speed and accuracy of docking with a new scoring function, efficient optimization, and multithreading. *Journal of Computational Chemistry* 31 (2): 455-461. doi: 10.1002/jcc.21334
- Tse LV, Hamilton AM, Friling T, Whittaker GR (2014). A novel activation mechanism of avian influenza virus H9N2 by furin. *Journal of Virology* 88 (3): 1673-1683. doi: 10.1128/JVI.02648-13
- Vander Kooi CW, Jusino MA, Perman B, Neau DB, Bellamy HD et al. (2007). Structural basis for ligand and heparin binding to neuropilin B domains. *Proceedings of the National Academy of Sciences of the United States of America* 104 (15): 6152-6157. doi: 10.1073/pnas.0700043104

- Venkatagopalan P, Daskalova SM, Lopez LA, Dolezal KA, Hogue BG (2015). Coronavirus envelope (E) protein remains at the site of assembly. *Virology* 478: 75-85. doi: 10.1016/j.virol.2015.02.005
- Walls AC, Park YJ, Tortorici MA, Wall A, McGuire AT et al. (2020). Structure, function, and antigenicity of the SARS-CoV-2 spike glycoprotein. *Cell* 181 (2): 281-292. doi: 10.1016/j.cell.2020.02.058
- Wang JM (2020). Fast identification of possible drug treatment of coronavirus disease-19 (COVID-19) through computational drug repurposing study. *Journal of Chemical Information and Modeling* 60 (6): 3277-3286. doi: 10.1021/acs.jcim.0c00179
- Wang Q, Zhang Y, Wu L, Niu S, Song C et al. (2020). Structural and functional basis of SARS-CoV-2 entry by using human ACE2. *Cell* 181 (4): 894-904.e9. doi:10.1016/j.cell.2020.03.045
- Wishart DS, Knox C, Guo AC, Shrivastava S, Hassanali M et al. (2006). DrugBank: a comprehensive resource for in silico drug discovery and exploration. *Nucleic Acids Research* 34 (Database issue): D668-672. doi: 10.1093/nar/gkj067
- Wolfel R, Corman VM, Guggemos W, Seilmaier M, Zange S et al. (2020). Virological assessment of hospitalized patients with COVID-2019. *Nature* 581 (7809): 465-469. doi: 10.1038/s41586-020-2196-x
- Wrapp D, Wang NS, Corbett KS, Goldsmith JA, Hsieh CL et al. (2020). Cryo-EM structure of the 2019-nCoV spike in the prefusion conformation. *Science* 367 (6483): 1260-1263. doi: 10.1126/science.abb2507
- Wu A, Peng Y, Huang B, Ding X, Wang X et al. (2020a). Genome composition and divergence of the novel coronavirus (2019-nCoV) originating in China. *Cell Host & Microbe* 27 (3): 325-328. doi: 10.1016/j.chom.2020.02.001
- Wu CR, Liu Y, Yang YY, Zhang P, Zhong W et al. (2020b). Analysis of therapeutic targets for SARS-CoV-2 and discovery of potential drugs by computational methods. *Acta Pharmaceutica Sinica B* 10 (5): 766-788. doi:10.1016/j.apsb.2020.02.008
- Wu F, Zhao S, Yu B, Chen YM, Wang W et al. (2020c). A new coronavirus associated with human respiratory disease in China. *Nature* 580 (7803): E7. doi: 10.1038/s41586-020-2202-3
- Yan R, Zhang Y, Li Y, Xia L, Guo Y et al. (2020). Structural basis for the recognition of SARS-CoV-2 by full-length human ACE2. *Science* 367 (6485): 1444-1448. doi: 10.1126/science.abb2762
- Yi Y, Lagniton PNP, Ye S, Li E Q, Xu RH (2020). COVID-19: what has been learned and to be learned about the novel coronavirus disease. *International Journal of Biological Sciences* 16 (10): 1753-1766. doi: 10.7150/ijbs.45134
- Yoshimoto FK (2020). The Proteins of Severe Acute Respiratory Syndrome Coronavirus-2 (SARS CoV-2 or n-COV19), the Cause of COVID-19. *Protein Journal* 39 (3): 198-216. doi: 10.1007/s10930-020-09901-4
- Zhang H, Kang Z, Gong H, Xu D, Wang J et al. (2020). The digestive system is a potential route of 2019-nCov infection: a bioinformatics analysis based on single-cell transcriptomes. *bioRxiv*. doi: 10.1101/2020.01.30.927806
- Zhou P, Yang XL, Wang XG, Hu B, Zhang L et al. (2020). A pneumonia outbreak associated with a new coronavirus of probable bat origin. *Nature* 579 (7798): 270-273. doi: 10.1038/s41586-020-2012-7

Table S1. Top 100 drugs from docking simulations.

Vina binding energy (kcal/mol)	ZINC ID	Drug name	Usage
-8.5	ZINC000011679756	Eltrombopag	Used to treat low blood platelet counts in adults with chronic immune (idiopathic) thrombocytopenia (ITP)
-8.5	ZINC000003830767	Estradiol benzoate	Act as the major female sex hormone
-8.5	ZINC000019632618	Imatinib	A small molecule kinase inhibitor used to treat certain types of cancer.
-8.4	ZINC000064033452	Lumacaftor	Used for the management of Cystic Fibrosis (CF) in patients aged 6 years and older.
-8.4	ZINC000011681563	Netupitant	An antiemetic drug used in combination with palonosetron for the prevention of acute and delayed vomiting and nausea associated with cancer chemotherapy
-8.4	ZINC000036701290	Ponatinib	Ponatinib is a novel Bcr-Abl tyrosine kinase inhibitor that is especially effective against the T315I mutation for the treatment of chronic myeloid leukemia.
-8.3	ZINC000000006157	Epinastine	Used for the prevention of itching associated with allergic conjunctivitis.
-8.3	ZINC000000002070	Sorbinil	Aldose reductase inhibitor
-8.2	ZINC000000537791	Glimepiride	Used for the management of type 2 diabetes mellitus (T2DM) to improve glycemic control.
-8.2	ZINC000003932831	Dutasteride	Novel dual 5 α -reductase inhibitor that works by blocking both isoforms of 5 α -reductase enzymes in a potent, selective, and irreversible manner.
-8.2	ZINC000001489478	Sitagliptin	A Dipeptidyl peptidase-4 (DPP-4) inhibitor used in conjunction with diet and exercise to improve glycemic control in patients with type 2 diabetes mellitus
-8.2	ZINC000000004724	Trileptal	An antiepileptic medication used in the treatment of partial onset seizures that was first approved for use in the United States in 2000
-8.1	ZINC000001996117	Darifenacin	Used to treat urinary incontinence.
-8.1	ZINC000052955754	Ergotamine	Alpha-1 selective adrenergic agonist and is commonly used in the treatment of migraine disorders.
-8.1	ZINC000002032615	Permethrin	A pyrethroid insecticide commonly used in the treatment of lice infestations and scabies.
-8.1	ZINC000003831448	Silibinin	Has hepatoprotective (antihepatotoxic) properties that protect liver cells against toxins.
-8	ZINC000000119978	Catechin	An antioxidant flavonoid
-8	ZINC000003869855	Dicumarol	Interferes with the metabolism of vitamin K.
-8	ZINC000003978005	Dihydroergotamine	A 9,10 α -dihydro derivative of ergotamine. It is used as a vasoconstrictor, specifically for the therapy of migraine disorders.
-8	ZINC000003830847	Flubendazole	Flubendazole is an anthelmintic that is used to treat worm infection in humans.
-8	ZINC000000897089	Mefloquine	A phospholipid-interacting antimalarial drug.
-8	ZINC000001540998	Pemetrexed	Use in combination with cisplatin for the treatment of patients with malignant pleural mesothelioma
-8	ZINC000002510358	Phenytoin	One of the most commonly used anticonvulsants.
-8	ZINC000001539579	Targretin	An antineoplastic agent used off-label for lung cancer, breast cancer, and Kaposi's sarcoma.
-7.9	ZINC000012504271	Atovaquone	A hydroxynaphthoquinone, or an analog of ubiquinone, that has antimicrobial and antipneumocystis activity.
-7.9	ZINC000003830772	Estradiol cypionate	Major female sex hormone.
-7.9	ZINC000003824921	Fexofenadine	Antihistamine used in the treatment of various allergic symptoms
-7.9	ZINC000002036732	Florantyrone	Florantyrone is used in the treatment of biliary dyskinesia

Table S1. (Continued.)

Vina binding energy (kcal/mol)	ZINC ID	Drug name	Usage
-7.9	ZINC00000002272	Ketoprofen	A nonsteroidal antiinflammatory agent (NSAIA) with analgesic and antipyretic properties
-7.9	ZINC000003831159	Latamoxef	A broad- spectrum beta-lactam antibiotic
-7.9	ZINC000000121541	Mebendazole	Acts by interfering with carbohydrate metabolism and inhibiting polymerization of microtubules.
-7.9	ZINC000003831169	Nafcillin	A semisynthetic antibiotic related to penicillin
-7.9	ZINC000003816514	Rolapitant	A potent, highly selective, long-acting neurokinin-1 (NK-1) receptor antagonist
-7.9	ZINC000000004785	Tegretol	Used to control seizures and to treat pain resulting from trigeminal neuralgia
-7.8	ZINC000000896717	Zafirlukast	An oral leukotriene receptor antagonist (LTRA) for the maintenance treatment of asthma
-7.8	ZINC000000009073	Apomorphine	A nonergoline dopamine D2 agonist indicated to treat hypomobility associated with Parkinson's.
-7.8	ZINC000000968264	Cyproheptadine	A serotonin antagonist and a histamine H1 blocker used as antipruritic
-7.8	ZINC000003830628	Danazol	A synthetic steroid with antigonadotropic and antiestrogenic activities
-7.8	ZINC000003830765	Estradiol	Estradiol is a naturally occurring hormone circulating endogenously in females.
-7.8	ZINC000003939013	Fosaprepitant	An intravenously administered antiemetic drug.
-7.8	ZINC000005162311	Ilevro	A nonsteroidal antiinflammatory prodrug (NSAID)
-7.8	ZINC000000002279	Ketorolac	A nonsteroidal antiinflammatory drug (NSAID)
-7.8	ZINC000003831231	Novobiocin	An antibiotic compound derived from <i>Streptomyces niveus</i> .
-7.8	ZINC000000897253	Olopatadine	Selective histamine H1 antagonist and mast cell stabilizer
-7.8	ZINC000004175630	Pimozide	An antipsychotic agent, alternative to haloperidol for the suppression of vocal and motor tics in patients with Tourette syndrome.
-7.8	ZINC000000538658	Tolvaptan	Used to treat low blood sodium levels (hyponatremia) associated with various conditions
-7.8	ZINC000006745272	Regorafenib	Regorafenib is an orally-administered inhibitor of multiple kinases.
-7.8	ZINC000000020253	Thalitone	A thiazide-like diuretic used for the treatment of hypertension
-7.7	ZINC000003830716	Diphenoxylate	A meperidine congener used as an antidiarrheal
-7.7	ZINC000027428713	Aprepitant	An antiemetic, P/neurokinin 1 (NK1) receptor antagonist
-7.7	ZINC000000537795	Glipizide	An oral hypoglycemic agent, used to control blood sugar levels in patients with type 2 diabetes mellitus.
-7.7	ZINC000019796080	Droperidol	Used in conjunction with an opioid analgesic such as fentanyl to maintain the patient in a calm state of neuroleptanalgesia
-7.7	ZINC000001550477	Lapatinib	An anticancer drug
-7.7	ZINC000000000509	Mirtazapine	A tetracyclic piperazino-azepine antidepressant agent
-7.7	ZINC000004213946	Nebivolol	A racemic mixture of 2 enantiomers where one is a beta adrenergic antagonist and the other acts as a cardiac stimulant without beta adrenergic activity.
-7.7	ZINC000001481956	Paliperidone	The primary active metabolite of risperidone
-7.7	ZINC000003819392	Riociguat	A soluble guanylate cyclase (sGC) agonist
-7.7	ZINC000001493878	Sorafenib	Used for the treatment of advanced renal cell carcinoma (primary kidney cancer).
-7.7	ZINC000004475353	Sulindac	A nonsteroidal antiinflammatory drug (NSAID) of the arylalkanoic acid class
-7.7	ZINC000003831615	Zeranol	A nonsteroidal estrogen agonist.

Table S1. (Continued.)

Vina binding energy (kcal/mol)	ZINC ID	Drug name	Usage
-7.7	ZINC000000538550	Ziprasidone	Atypical antipsychotics, used to treat schizophrenia and bipolar disorder
-7.6	ZINC000002568036	Dantrolene	A hydantoin derivative but does not exhibit antiepileptic activity
-7.6	ZINC000000403011	Labetalol	Used to treat hypertension
-7.6	ZINC000053151228	Methysergide	An ergot derivative that antagonizes the effects of serotonin in blood vessels and gastrointestinal smooth muscle
-7.6	ZINC000001530977	Naftifine	A synthetic, broad spectrum, antifungal agent
-7.6	ZINC000084589076	Warfarin	An anticoagulant drug normally used to prevent blood clot formation as well as migration.
-7.6	ZINC000000523926	Gliclazide	Used for the treatment of noninsulin-dependent diabetes mellitus (NIDDM).
-7.6	ZINC000003831490	Sulfasalazine	Used in the management of inflammatory bowel diseases.
-7.6	ZINC000001530596	Cephalexin	Used to treat a number of susceptible bacterial infections through inhibition of cell wall synthesis
-7.6	ZINC000001552174	Cilostazol	Quinolinone derivative and antiplatelet agent with vasodilating properties
-7.6	ZINC000000402909	Fenoprofen	An antiinflammatory analgesic and antipyretic highly bound to plasma proteins.
-7.6	ZINC000000537877	Ketanserin	Investigated for the treatment of septic shock, severe sepsis, and diabetic foot ulcer.
-7.6	ZINC000003830435	Ceforanide	Second-generation cephalosporin antibiotic
-7.6	ZINC000058581064	Dolutegravir	HIV-1 integrase inhibitor
-7.6	ZINC000013520815	Estradiol Transdermal Patch	Naturally occurring hormone circulating endogenously in females. Used in several hormone therapy products for managing conditions associated with reduced estrogen
-7.6	ZINC000000000903	Alprazolam	Used for the treatment of anxiety and panic disorders.
-7.6	ZINC000000538505	Trifluoperidol	Experimental
-7.6	ZINC000001997125	Pomalidomide	An immunomodulatory antineoplastic agent
-7.6	ZINC000053683151	Bromocriptine	A semisynthetic ergot alkaloid derivative with potent dopaminergic activity.
-7.6	ZINC000003802417	Alvimopan	Peripherally acting μ opioid antagonist.
-7.6	ZINC000000537804	Glisoxepide	sulphonamide-derived oral antidiabetic drug
-7.6	ZINC000009212426	Leucovorin	A necessary cofactor in the body.
-7.6	ZINC000001481983	Benzocetamine	Used as a sedative which does not depress the respiratory system, but rather stimulates it.
-7.6	ZINC000001612996	Irinotecan	Anticancer
-7.6	ZINC000000968337	Azatadine	Antihistamines to compete with histamine for histamine H1- receptor sites on effector cells.
-7.6	ZINC000019632668	Doxapram	A central respiratory stimulant with a brief duration of action
-7.6	ZINC000003830594	Dicloxacillin	One of the penicillins which is resistant to penicillinase
-7.6	ZINC000003830401	Cefatrizine	Experimental
-7.6	ZINC000068202099	Sonidegib	A Hedgehog signaling pathway inhibitor developed as an anticancer agent.
-7.6	ZINC000000057321	Fenoterol	An adrenergic beta-2 agonist that is used as a bronchodilator and tocolytic.
-7.5	ZINC000000086535	Flufenamic acid	An anthranilic acid derivative with analgesic, antiinflammatory, and antipyretic properties.
-7.5	ZINC000018067894	Acetohexamid	A sulfonylurea hypoglycemic agent

Table S1. (Continued.)

Vina binding energy (kcal/mol)	ZINC ID	Drug name	Usage
-7.5	ZINC000000897225	Hidroflumetiazid	A thiazide diuretic with actions and uses similar to those of hydrochlorothiazide
-7.5	ZINC000043207238	Canagliflozin	A sodium-glucose cotransporter 2 (SGLT2) inhibitor used in the management of type 2 diabetes mellitus
-7.5	ZINC000000897408	Bicalutamide	An oral nonsteroidal antiandrogen for prostate cancer.
-7.5	ZINC000000004893	Asenapine	Atypical antipsychotic for treatment of schizophrenia and acute mania associated with bipolar disorder.
-7.5	ZINC000035342789	Tolcapone	Used in the treatment of Parkinson's disease as an adjunct to levodopa/carbidopa medication.
-7.5	ZINC000019796168	Sildenafil	Prevents or minimizes the breakdown of cyclic guanosine monophosphate (cGMP) by inhibiting cGMP specific phosphodiesterase type 5 (PDE5) pulmonary hypertension
-7.5	ZINC000003830836	Doxepin	A psychotropic agent with antidepressant and anxiolytic properties
-7.5	ZINC000000001547	Hydroxystilbamidine isethionate	Used in the therapy of some patients with nonprogressive blastomycosis of the skin, and pulmonary or systemic blastomycosis in children

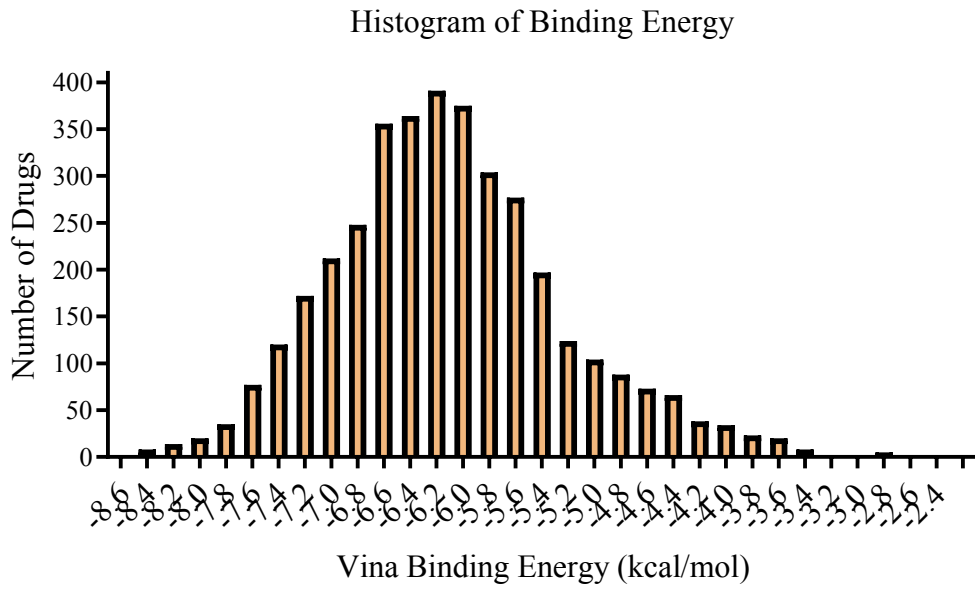


Figure S1. Vina binding energies of all drugs to NRP1.